

Construction of a Dye Laser for Use in Detecting Ultracold RbCa

Hayley Whitson

Willamette University Physics Department

Advised by Professor Michaela Kleinert

May 8, 2012

Abstract

Ultracold heteronuclear molecules have seen increasing interest in the scientific community over the last few years. By controlling their ro-vibrational energy levels, ultracold molecules can be used for high precision spectroscopy, to study cold collisions with rich internal dynamics, as model systems for condensed matter physics, and as qubits in quantum information processing. We study the novel combination RbCa. In addition to a permanent electric dipole moment, it also possesses a permanent magnetic dipole moment. This makes it an ideal candidate to study strong long-range dipole-dipole interactions.

This thesis outlines the construction of a dye laser system which will be used to ionize RbCa through resonantly enhanced multi-photon ionization (REMPI). We use a Nd:YAG pulsed laser to pump a dye solution, Rhodamine 590 in methanol, contained in a quartz glass cell. The linewidth of the dye laser is narrowed through use of a diffraction grating in Littman-Metcalf configuration. We have performed *ab initio* calculations to calculate the electronic energy levels of RbCa, and Franck-Condon factors to determine the best wavelength for REMPI. These data will be used to optimize further calculations of molecular energy levels.

Contents

1	Introduction	1
2	Lasers	3
2.1	Basic Laser Structure	4
2.1.1	Energy Source, Absorption, and Emission	4
2.1.2	Resonance Cavity	6
2.2	Population Inversion	6
3	Pump Laser	8
3.1	Theory of a Nd:YAG Pulsed Laser	9
3.1.1	Laser Medium	9
3.1.2	Frequency Doubling	10
3.1.3	Q-Switching	14
3.2	Characterization of the Pump Light	15
3.2.1	Beam Profile and Crystal Optimization	16
3.2.2	Pulse Width	21
3.2.3	Power Output	24
4	Dye Laser	26
4.1	A Theoretical Understanding	26
4.1.1	Dye Molecules	26
4.1.2	Laser Cavity	30
4.2	Cavity Construction	32
4.3	Characterization of the Dye Laser	34
5	Application and Outlook	37
5.1	Ionization of Ultracold RbCa	37
5.2	Franck Condon Principle	40

List of Figures

1	Metaphor for ultracold physics	2
2	Absorption and the two different emission types	5
3	Allowed and disallowed modes of a resonance cavity	6
4	Diagram of a two level lasing system	7
5	Three and four level laser diagrams	8
6	Energy levels of a Nd:YAG crystal	10
7	Second harmonic generation	11
8	Unpolarized light traveling through a birefringent material	12
9	Phase matching of two waves	13
10	Q-Switch diagram	14
11	Electro-optical Q-Switch	15
12	Nd:YAG laser in operation	16
13	Gaussian profile in DataRay	17
14	Crystal temperature controller	18
15	Temperature optimization of K*DP crystal	19
16	Power data for crystal temperature optimization	20
17	Pulse of Nd:YAG in long pulse setting	22
18	Pulse of Nd:YAG in Q-Switched mode	23
19	Pulse width of the Nd:YAG versus repetition rate	24
20	Average power of long pulse and Q-SW modes	25
21	Molecular structure of Rhodamine 590	26
22	Broad shape of energy levels of a molecule	28
23	Focusing the pump beam on the dye cell	29
24	Tilting the dye cell away from vertical	30
25	Littman and Metcalf cavity design	31
26	Tuning mirror	32
27	Picture of our dye laser cavity	33
28	Entire setup	34
29	Relative power vs. wavelength measured on a pulsed power meter	35
30	Relative power vs. wavelength measured on a spectroscope	36
31	Pulse shape of the dye laser measured on the specroscope	37
32	REMPI	38
33	Example of results from a similar experiment	40
34	The wavefunctions of a molecule's ground and excited states	42

35	Energy levels of RbCa	43
36	Density plots of Franck-Condon factors for RbCa . . .	44

List of Tables

1	Average power measurements for Long Pulse and Q-SW modes	25
2	Largest Franck-Condon factors	46

1 Introduction

In 1924, a thirty-year old physics professor by the name of Satyendra Bose sent Albert Einstein his paper on light quanta (now known as photons). The paper, entitled “Planck’s Law and the Hypothesis of Light Quanta,” intrigued Einstein who in turn considered how atoms would behave if they followed the same physical rules as photons [1]. He predicted that at extremely low temperatures, particles within a gas of atoms would all condense into the lowest quantum energy state possible. This new state of matter would have different properties from any other form of matter ever previously observed. In 1995, a little over seventy years after Einstein’s prediction, physicists at the Joint Institute of Laboratory Astrophysics in Boulder, Colorado used a MOT¹ to create a Bose-Einstein condensate of rubidium atoms at 200 billionths of a degree above absolute zero [3]. This discovery was given the Nobel Prize in Physics in 2001. This ground-breaking experiment is what has paved the way for the new fields of cold and ultracold physics and chemistry.

Why are ultracold methods such great ways to study atoms and molecules? Imagine standing on a sidewalk watching traffic go by. As the cars pass, their speed gives you only a fraction of a second to determine characteristics about the car. Now imagine a car parked in your driveway; you can walk around it, study it from different angles, and maybe even lift the hood to understand the mechanisms that make the car run. As atoms and molecules are constantly moving at very large speeds (several 100’s to 1000’s of meters per second) studying them is like attempting to study details on a car speeding down the highway (Figure 1). If this matter could somehow be “parked,” then this could lead to a better understanding of the qualities that give the quantum regime its structure. This is what ultracold research has been able to achieve.

¹William Phillips, Claude Tannoudji, and Steven Chu created the first magneto-optical trap (MOT) which was awarded the 1997 Nobel Prize in Physics [2].



Figure 1: A car that is speeding down the highway is much harder to see details on than a parked car. The parked car gives an opportunity to study the details close up. This is much like how trapping atoms using ultracold techniques gives opportunity for studying a molecule's characteristics much more easily than at higher temperatures.

Temperature is a measure of kinetic energy. More specifically, the equation,

$$k_B T = mv^2. \quad (1)$$

relates the temperature, T , of an ensemble of molecules to its average kinetic energy, mv^2 , through the Boltzmann's constant, k_B . However, within the MOT the density is extremely low and averaging is no longer possible. Thus, by cooling these molecules to temperatures very close to absolute zero, any kinetic movements are essentially stopped and the structure and characteristics of the molecules can be focused on [4].

The research discussed in this paper aims to study the heteronuclear diatomic molecule, rubidium calcium (RbCa), which has never been created in the lab before. The important properties of RbCa are its permanent electric and magnetic dipole moments. With these properties, strong long-range dipole-dipole interactions can be studied, leading to an extremely novel possible application, quantum computation [5]. The long-range interactions offer “a means for controlled creation of entangled states” [5]. Because of the superposition principle, a quantum computer will have more processing ability than a classical computer. For example, in evaluating a function f , the answer will be transferred in a superposition of all possible answers but result in one answer when the measurement is observed [6]. These computers will, in theory, be able to compute more difficult problems and work faster overall. As today’s world runs on computers, this will be extremely beneficial in an almost infinite number of ways. Other studies and applications of ultracold molecules include advances in

precision measurements, novel quantum degenerate systems, explorations in ultracold chemistry, and tests of fundamental symmetries [4, 5].

In order to harness the potential of these molecules for technological advances, it is necessary to be able to control or predict how many molecules and in which quantum state they will be created in. Using a computer program predictions can be made from known data about the energy levels of Rb and Ca atoms, however *ab initio* calculations are difficult as the system we are attempting to describe is extremely complex. Thus, the state the molecule will be created in cannot be predicted accurately. In fact, this is one measurement our research hopes to solidify. By using experimental data our computer models can be improved and vice versa. Alternating between theory and experiment results in a better understanding of these molecules and is an essential step towards their use in future applications. The research in this paper contributes to this understanding by outlining the construction of a dye laser system which can ionize ultracold molecules, making it easier and more efficient to detect them while gaining information about the original energetic configuration of the molecule. It was built in the lab of Professor Michaela Kleinert while she simultaneously worked on cooling rubidium and calcium in their respective magneto-optical traps. After the atoms are cooled, they will be formed into a molecule using a process known as photoassociation. And once the molecules are formed, the dye laser system will be used to study them (see section 5.1 for more information on the application of the dye laser).

Discovered in 1966 by Sorokin and Larkin, dye lasers have many features that make them useful for physics research [7]. They are tunable over a large range of wavelengths from the visible to the infrared, have a range of possible output powers, and can be continuous wave or pulsed lasers. An outline of basic laser components followed by the in-depth theory and methods of the pump and dye laser will comprise the next three sections. This is followed by a section discussing the future outlook of this project.

2 Lasers

Lasers are seen in a variety of practical uses in society today. Their properties are extremely useful in applications within medicine, com-

munications, industry, research and many others [8]. Lasers, an acronym standing for *Light Amplification by Stimulated Emission of Radiation*, convert energy into coherent light. Coherence is a property of waves, in this case electromagnetic waves, which is defined by a consistent phase relation and frequency between multiple waves. The three main parts of a laser that give the output light this nature are an energy source (the pump source), a medium, and a resonance cavity. There are numerous other parts one can add to the system to change or control the spatial or temporal nature of the coherence, some of which will be addressed in the construction of the dye laser. In this section I will only discuss the three basic parts necessary for lasing.

2.1 Basic Laser Structure

2.1.1 Energy Source, Absorption, and Emission

The energy supplied to a laser can occur in the form of an electromagnetic wave (light). This pump light is absorbed by the lasing medium (a gas, liquid or solid substance made of atoms or molecules that can be excited easily). The absorption results in the excitation of electrons to higher energy levels within the atoms or molecules (Figure 2(a)).

Because it is energetically favorable for the electron to exist in the ground state, when it is in a higher state it will decay to a lower one repeatedly until it is in the ground state. When electrons decay, the energy between the two levels must be conserved. This energy can be released through heat or the emission of photons. Lasers are a result of the latter. There are two types of emission, spontaneous and stimulated. Spontaneous emission (Figure 2(b)) is when the transition between two energy levels occurs as the emission of a photon without an external mechanism, or *spontaneously*, thus the name. This photon will have energy equal to the difference between the energy levels where the transition occurred,

$$h\nu = E_2 - E_1 . \quad (2)$$

However, because this photon is emitted spontaneously, it will be emitted with a random direction and phase. Thus, most spontaneously emitted photons will destructively interfere.

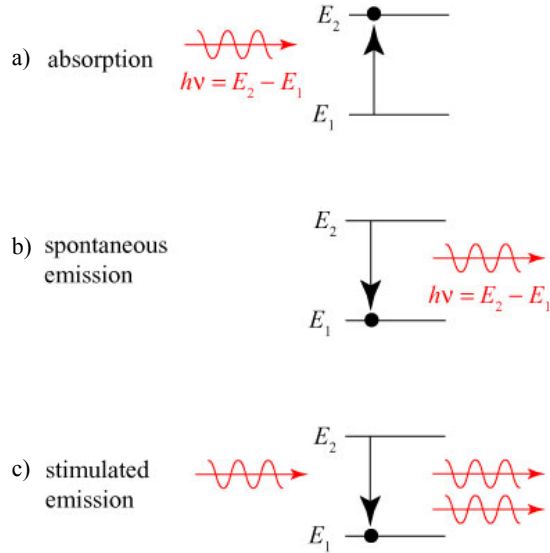


Figure 2: Photons incident on an atom or molecule can be absorbed which excites an electron to a higher energy level (a). Once an electron is in a higher energy state, it can decay to a lower energy level spontaneously (b) or by an external photon stimulating the transition (c). Stimulated emission is essential for lasing to occur [9].

Stimulated emission differs because external photons cause the transition between energy levels to occur (Figure 2(c)). In order for a photon to stimulate the transition, it must have energy equal to the difference between the energy levels,

$$h\nu_1 = E_2 - E_1 . \quad (3)$$

And, because the stimulated photon will have this energy as well,

$$h\nu_2 = E_2 - E_1 = h\nu_1 \quad (4)$$

the overall outgoing intensity is twice that of the original photon,

$$h\nu_1 + h\nu_2 = 2 * h\nu_1 . \quad (5)$$

The emitted photon will have the same frequency, direction, and phase as the external photons. Essentially, the emitted photon will be a clone of the original, and the two photons will move together through space as coherent light.

2.1.2 Resonance Cavity

The resonance cavity assists in the magnification of stimulated emission. It provides a way for the coherent photons to multiply in number. A geometry can be created using mirrors that will reflect the beam repeatedly back and forth through the medium stimulating new photons on each pass. This is called a resonance cavity because the emitted light will create standing waves within the cavity (Figure 3). The allowed modes of the cavity depend on its length. To create the output beam, one of the mirrors is partially transmissive.

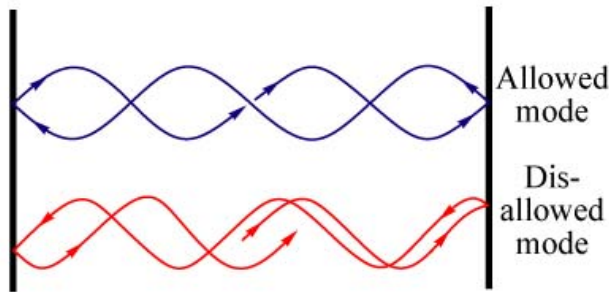


Figure 3: The allowed and disallowed modes of a resonance cavity depend on the length of the cavity. The resonant waves will be standing waves [10].

2.2 Population Inversion

A necessity for the success of a laser system is the creation of a population inversion between energy levels. The population of an energy level, N_i , is the number of molecules or atoms in the i^{th} energy level. The rates of stimulated emission and of absorption are proportional to the population of the excited and ground states, respectively, as well as the intensity of the incoming light source. Thus, if the excited state has a higher population than the ground state, there will be more stimulated emission than absorption and vice versa. A laser requires more stimulated emission than absorption within the laser because otherwise there would be no amplification within the cavity, or no net gain. Therefore, the population ratio must be $\frac{N_e}{N_g} > 1$ for lasing. This phenomenon is known as population inversion.

With a two level system, this can never be achieved because the energy levels will, at best, achieve an equilibrium of electrons between

the two states and will solely trade an electron back and forth, always sustaining the equilibrium. Suppose a population, N_2 , is in the E_2 energy level with an incoming electromagnetic energy source. Within this two level process, the population of E_2 depends on three factors. The population will decrease over time due to spontaneous emission at a rate, A , proportional to N_2 ,

$$\frac{dN_2(t)}{dt} = -AN_2. \quad (6)$$

Simultaneously, the N_2 population is growing through absorption at a rate B_{12} ,

$$\frac{dN_2(t)}{dt} = \lambda B_{12}N_1 \quad (7)$$

where λ is a factor proportional to the light field. And, the third factor, stimulated emission, decreases the population of N_2 as,

$$\frac{dN_2(t)}{dt} = -\lambda B_{21}N_2. \quad (8)$$

Figure 4 shows a diagram of this process.

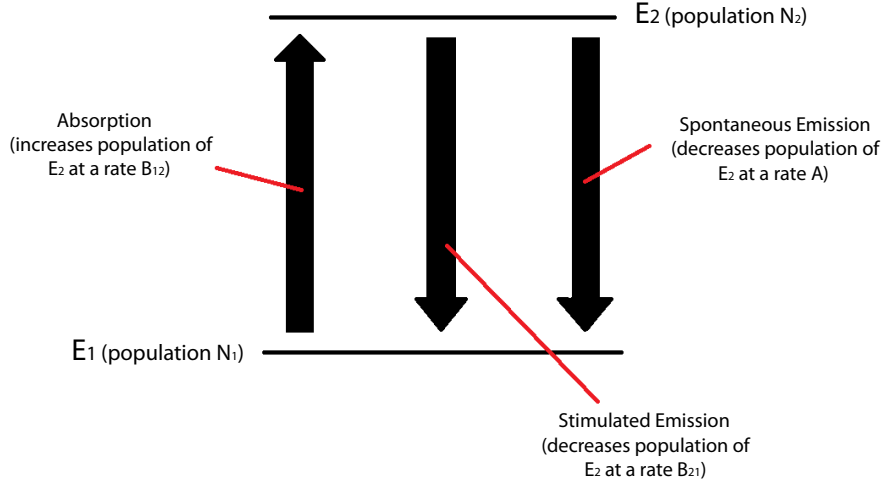


Figure 4: A two level lasing system with energy levels E_1 and E_2 with populations N_1 and N_2 , respectively. Three factors, each with an associated rate, contribute to how the population of E_2 changes with time. The three factors are absorption, stimulated emission, and spontaneous emission.

Adding these contributions up yields

$$\frac{dN_2(t)}{dt} = -AN_2 + \lambda B_{12}N_1 - \lambda B_{21}N_2. \quad (9)$$

And, because stimulated emission and absorption are inverse processes,

$$B_{12} = B_{21} = B$$

and equation (9) becomes

$$\frac{dN_2(t)}{dt} = -AN_2 + \lambda B(N_1 - N_2). \quad (10)$$

In order for stimulated emission to be more likely than absorption, N_2 must be greater than N_1 . Now suppose this is true, that $N_2 > N_1$. Then the overall population of N_2 is decreasing ($\frac{dN_2(t)}{dt} < 0$). Thus, this situation can never achieve gain.

Three or four level pumping schemes will achieve better results because having a third or fourth energy level will provide a place for electrons to build (Figure 5). The transitions with short lifetimes will decay quickly, but there needs to be an intermediate level in which the lifetime is long. Because of this time delay, a population can build creating the inversion.

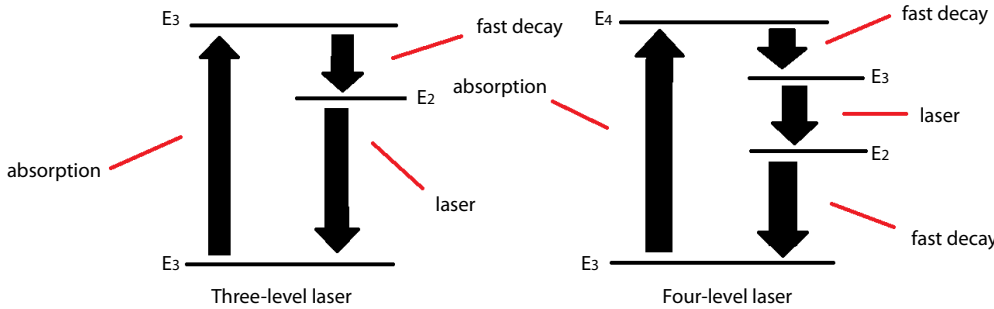


Figure 5: Three and four level laser systems, unlike a two level system, have an energy level in which a population inversion can build.

3 Pump Laser

The second harmonic (532 nm) of a Spectra Physics Quanta-Ray GCR Series12S pulsed laser system is used as the pump laser for the dye

laser. The Quanta Ray is a Nd:YAG (neo-dymium yttrium aluminium garnet) laser. Differing from continuous wave set up, pulsed lasers will emit a pulse of light for a short duration at some repetition rate. This allows more power to be built up between emissions, and thus a short powerful pulse can result (see Q-Switching Section 3.1.3). The pump source used in this experiment is a pulsed Nd:YAG laser system. This results in a pulsed output beam from the dye laser. We choose to use 532 nm because the conversion efficiency of this type of pump light into a laser from the dye is higher ($\sim 30 - 40\%$) compared to uv light ($\sim 10\%$) [11].

3.1 Theory of a Nd:YAG Pulsed Laser

3.1.1 Laser Medium

Yttrium aluminum garnet (YAG) is a crystalline structure that acts as the medium for the Nd:YAG laser, thus the name. This crystal is pumped by a flashlamp, which excites electrons in the medium to a higher energy level. About 1 atomic percent of the Y^+ ions are replaced by Nd^{3+} ions which is fairly easy considering these ions are similar in size [11]. This doping aids the crystal in absorbing the pump light. Once the electrons have been excited to a higher energy level, they then spontaneously decay to the $\text{F}_{3/2}$ level where they stay for $\sim 230 \mu\text{sec}$ [12]. The most probable lasing transition will occur between this state and the $\text{I}_{11/2}$ state which corresponds to a laser beam with a wavelength of 1064 nm (Figure 6). Although other transitions are possible, “probability and wavelength-selective optics isolate the 1064 nm light” [12].

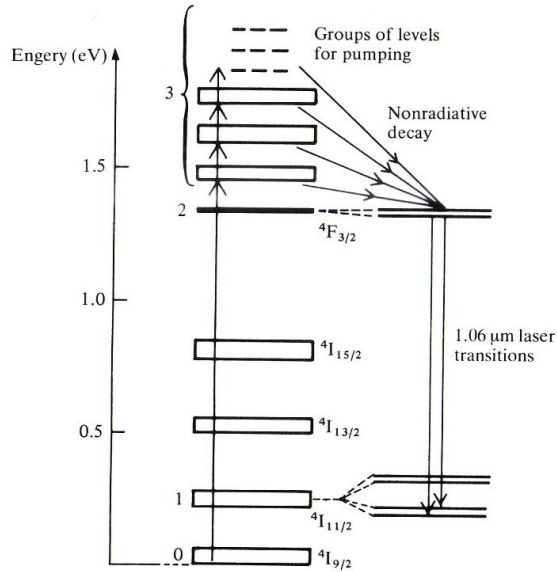


Figure 6: The energy levels of a Nd:YAG crystal along with the lasing transition from $F_{3/2}$ to $I_{11/2}$ which results in a laser with wavelength 1064 nm [13].

3.1.2 Frequency Doubling

When pumping the dye solution with a Nd:YAG laser system, 1064 nm is too long of a wavelength. There are no dyes that can be excited at this frequency. However, there are many dyes that can be pumped at 532 nm, the frequency doubled wavelength of 1064 nm [14]. Frequency doubling can occur when laser light enters a non-linear crystal. The optical properties of the crystal cause a beam with half the wavelength of the original beam to form (Figure 7).

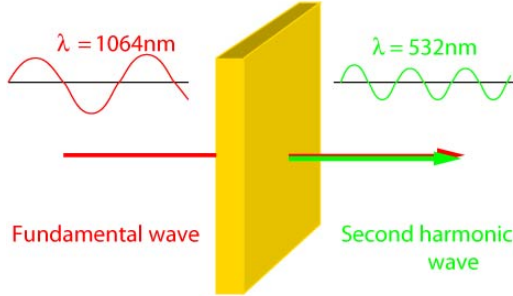


Figure 7: With an incident wavelength of 1064 nm, second harmonic generation through a non-linear crystal results in both the original beam and a beam of half the wavelength, or 532 nm [15].

Suppose an electromagnetic wave enters a crystal with an electric susceptibility of χ . At low intensities, the polarization of the crystal can be approximated as a linear relation,

$$P = \chi_1 E. \quad (11)$$

The electric field can be written as

$$E = E_0(e^{i\omega t} + e^{-i\omega t}) = 2E_0\cos(\omega t) \quad (12)$$

where E_0 is the amplitude, ω is the angular frequency of the electromagnetic wave, and t is time. However, when the intensity is large, for example in a pulsed laser, the non-linear term of the polarization becomes significant,

$$P = \chi_1 E + \chi_2 E^2. \quad (13)$$

The electric field squared is

$$\begin{aligned} |E^2| &= |E_0(e^{i\omega t} + e^{-i\omega t})|^2 = E_0^2 [(e^{i\omega t} + e^{-i\omega t})(e^{-i\omega t} + e^{i\omega t})] \\ &= E_0^2(2 + e^{2i\omega t} + e^{-2i\omega t}) = 2E_0^2 + 2E_0^2\cos(2\omega t) \end{aligned} \quad (14)$$

The second term of this is a wave with double the frequency (2ω) of the electromagnetic wave in the linear case. Thus, the original wave, once incident on the crystal, is the sum of two waves, a linear fundamental wave and a non-linear second harmonic wave. In high power pulsed laser systems like the Nd:YAG, the $|E^2|$ term dominates, resulting in a negligible linear term and higher conversion to the second harmonic wave. Also adding to this is specifically chosen crystals with

properties that make $\chi_2 \geq \chi_1$.

Another important contribution to the efficiency of frequency conversion is the crystal's birefringence. Normally, the index of refraction of a medium depends on the wavelength of the input beam, but there exist materials in which it also depends on the polarization of the beam. These materials are called birefringent materials. An anisotropy of binding forces between atoms in these crystals causes different indices of refraction. In the case of birefringence, two indices occur, one on two perpendicular axes and the other on the remaining axis. The axis with the unique index is known as the optical axis of the crystal and has an index of refraction, n_o , where o stands for ordinary. Light with polarization along this axis will follow the standard rules of refraction, which is reflected in the name *ordinary*. Light perpendicular to this axis will refract differently due to the extraordinary index of refraction, n_e . Unpolarized light will thus be split into two rays, the perpendicular polarization component will follow the optical axis with index n_o and the parallel component will refract differently with an index n_e (Figure 8)[16].

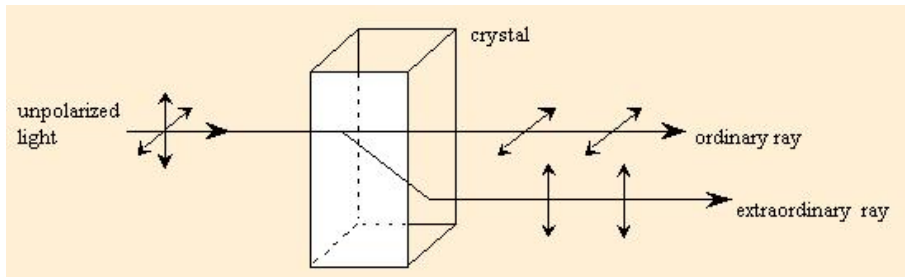


Figure 8: Unpolarized light when traveling through a non-linear birefringent material will result in two linearly polarized beams. This is due to the different indices of refraction along different axes of the crystal. This property can be used to phase-match the frequency doubled wave with the fundamental wave [16].

This property of the crystal assists in a process known as phase-matching. For maximal power conversion when frequency doubling, the speed and phase of both waves must be equal throughout the crystal. This insures any photon doubling in frequency will be in phase with the second harmonic wave. Otherwise destructive interference would occur resulting in lost power. This can be described with a

phase relation,

$$\Delta k = k_2 - 2k_1$$

where k_1 and k_2 are the phases of the fundamental and second harmonic waves, respectively. Because the phases need to be the same for maximum power conversion efficiency, a phase difference $\Delta k = 0$ is favorable (Figure 9).

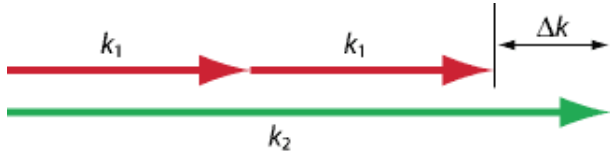


Figure 9: In order for efficient frequency doubling to occur, the phases of the fundamental and frequency doubled waves must be in phase ($\Delta k = 0$). This can be achieved through critical and non-critical phase matching techniques [17].

There are three types of phase matching, two are considered critical phase matching and the third is non-critical. The two critical phase matching techniques are called Type I and Type II, which each have a condition that must be satisfied. The conditions involve matching the angles of the ordinary and extraordinary components of the fundamental and frequency doubled waves in certain ways to maximize constructive interference. The conditions can be met by changing the angle the original wave enters the crystal. Non-critical phase matching is done by changing the temperature of the crystal. Because the indices of refraction have a temperature dependence, by increasing or decreasing the temperature, a phase matching condition can be met or critical phase matching can be improved. For a more complete description on phase matching see S. Hooker and C. Webb's *Laser Physics* [18].

The non-linear crystal used in the Nd:YAG system is KD*P (potassium dideuterium phosphate) [12]. KD*P is highly deuterated KDP, another common second harmonic generation crystal. KD*P is used in this laser as it has an absorbance percentage 11.667 times lower than KDP, thus resulting in much less power being lost into the crystal [19]. This reduction in absorbance also reduces the heat the absorbance would produce. Thus, it helps keep the temperature of the crystal stable.

3.1.3 Q-Switching

Although Nd:YAG lasers can be continuous wave lasers, to pump the dye laser a pulsed Nd:YAG system is used. This is because higher intensities can occur which aids in ionizing the RbCa molecules more efficiently. Normally, the lasing medium would emit light each time the flashlamp flashes. A technique that can be used to have more control over the pulse width and output the optimal power of pulsed lasers is called Q-switching. Q-switching increases the population inversion by inhibiting oscillation from occurring for a period of time. In this time the population inversion builds to far above the lasing threshold. The obstruction of oscillation is then stopped and the stored energy is released in a short, higher powered pulse. A high value of Q implies low energy loss in one oscillation cycle. Q-switching gets its name from this principle because Q-switching is repeatedly switching the Q -value of the system between high and low values. The Q -factor is defined by

$$Q = 2\pi * \frac{\text{energy stored}}{\text{energy lost in one oscillation cycle}} [11]. \quad (15)$$

The Nd:YAG laser used in this experiment uses an electro-optic Q-switch (Figure 10).

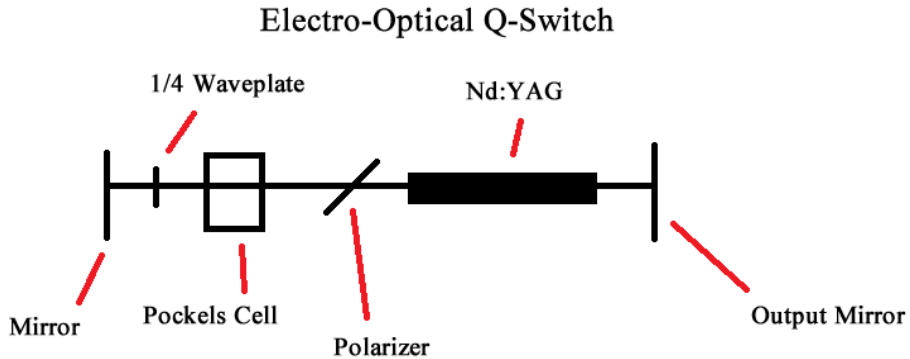


Figure 10: A diagram of the electro-optical Q-Switch inside the Nd:YAG pulsed laser system. Q-Switching gives the laser a greater amount of power on each pulse.

The Q-Switch switches the Q -factor between high and low by applying a voltage to the Pockels cell. Light entering the Q-switch is

first vertically polarized by the polarizer. With no voltage applied, the Pockels cell does not affect the light traveling through it. Thus, the beam travels to the quarter-wave plate which gives the beam a circular polarization. After being reflected off the high reflector (mirror) the quarter-wave plate converts the light to a horizontal polarization. The polarizer only transmits vertically polarized light so the beam is reflected away from the resonator cavity (Figure 11(a)). However, if a voltage is applied to the Pockels cell the horizontal polarization from the quarter-wave place is cancelled, the beam stays vertically polarized, and the light is transmitted into the resonance cavity (Figure 11(b))). The time the population inversion is building is $\sim 200\mu\text{sec}$ (the duration of the flashlamp pulse) at which point a high voltage is applied to the Pockels cell which quickly changes the Q-factor and releases a pulse with peak power on the order of tens of megawatts and with a pulse width less than 10 nsec.

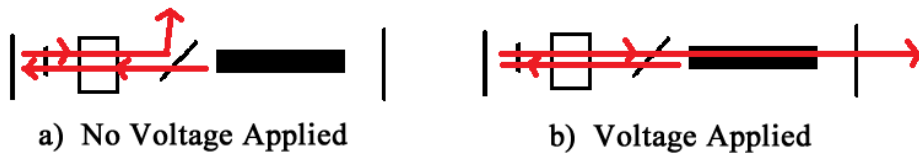


Figure 11: When no voltage is applied to the Pockels cell within the Q-Switch, the lasing is deflected from entering the resonator cavity. But if a short burst of voltage is applied, the beam is let through and results in a short powerful pulse from the laser.

3.2 Characterization of the Pump Light

In order to successfully build and characterize the dye laser, it was necessary to have as much information as possible about the pump laser. This information includes the pulse width, power output, and fluctuations in this power output. Thus, characterization of the Nd:YAG system was the first step in the creation of the dye laser. Because we are only interested in the 532 nm light for use in pumping the dye solution, we separated the 1064 nm and 532 nm light by using two longpass dichroic mirrors, both Thorlabs DMLP900, which transmit light at 932-1300 nm and reflect light at 400-872 nm with $\geq 90\%$ efficiency. By placing one 4 cm from the output of the laser at a 45° angle and another 26 cm away also at 45° , we reflected the 532 nm onto the optics table and filtered out the 1064 nm light. A picture of

the Nd:YAG laser light is shown in Figure 12. We characterized the pulse width and power output of this laser system in both the long pulse and Q-switched modes. We also optimized the power output by adjusting the settings of the second-harmonic generation crystal.

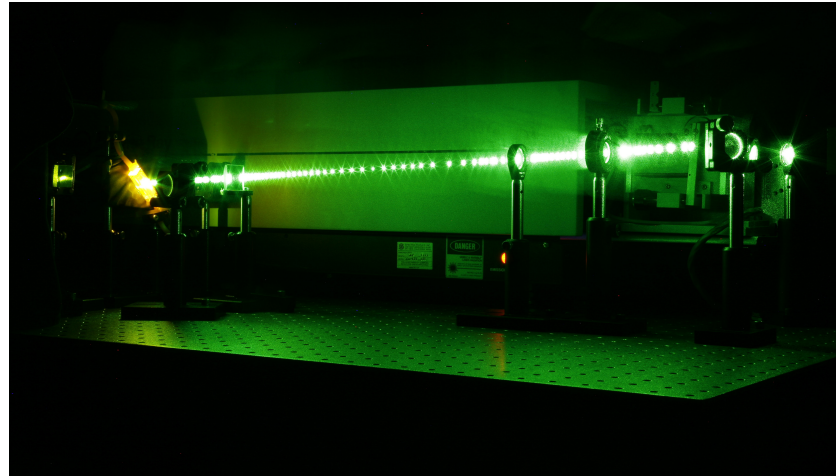


Figure 12: A picture of the Quanta Ray Nd:YAG laser in operation taken with a long exposure.

3.2.1 Beam Profile and Crystal Optimization

In order to have the most efficient power output, we want the laser beam to have a Gaussian shape, characterized by a bell shaped curve, where the power is most concentrated at the center and falling off at the edges (Figure 13).

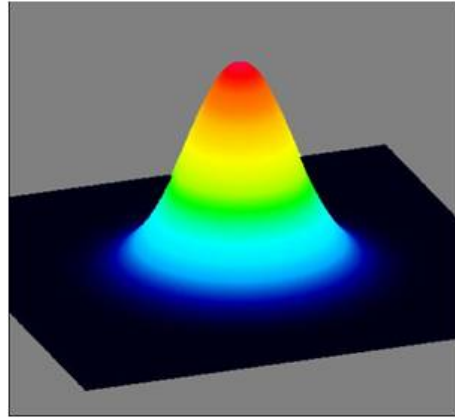


Figure 13: A Gaussian beam displayed in the DataRay program. This is what an ideal laser pulse would look like [20].

We tested this using Laser Beam Imaging software and WinCamD Series CCD camera by DataRay Inc. [20]. With this program we can create images and record the beam profile. There are many factors that can change the profile of the beam. As discussed in section 3.1.2, this includes the angle between the non-linear crystal and pump beam, polarization of the pump beam, and the temperature of the crystal. Using the DataRay software we monitored the changes in the beam profile as we adjusted one of these factors at a time. Thus, we optimized power output of the Nd:YAG laser by taking data as a function of one of the above factors and finding the optimal setting for each. Because the response of the laser was immediate when the polarization or the angle was changed, computer data was not necessary. However, when optimizing the temperature of the crystal collecting data was imperative, as it took the crystal housing 2-3 minutes to regulate the temperature once it was changed. To change the temperature setting, a screw in the crystal housing is turned clockwise or counter-clockwise to increase or decrease the temperature respectively (Figure 14).



Figure 14: A picture of the crystal temperature controller. To change the temperature, the screw is turned with a screwdriver. Turning the screw counter-clockwise decreases the temperature in the crystal housing and turning it clockwise increases it.

To take data, I designated the original position of the screw as 0 and a quarter turn clockwise as .25. Data points turned counter-clockwise from the starting point were deemed negative. I took data ranging from -4.5 turns to 4.5 turns. We averaged the DataRay peaks over 20 consecutive pulses for each temperature, used Origin to find the area of the peaks (as the area of intensity is proportional to power), plotted the areas versus temperature, and fitted a curve to find the optimal temperature of the crystal. The results of the temperature optimization are displayed in Figure 15.

The crystal angle and the incoming polarization of the 1064nm light were successfully optimized using the DataRay program. A noticeable increase in the height of the peaks occurred as the parameters were changed. The optimal position for both the polarization and the angle were met.

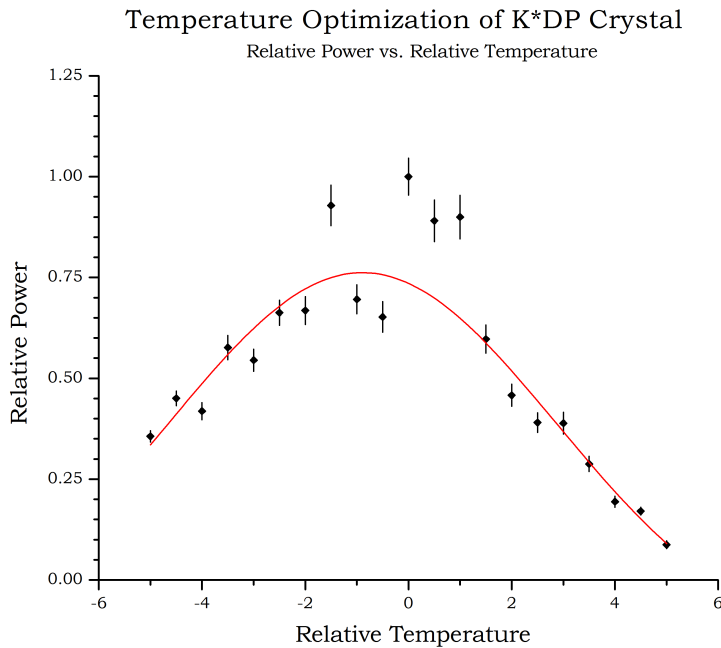
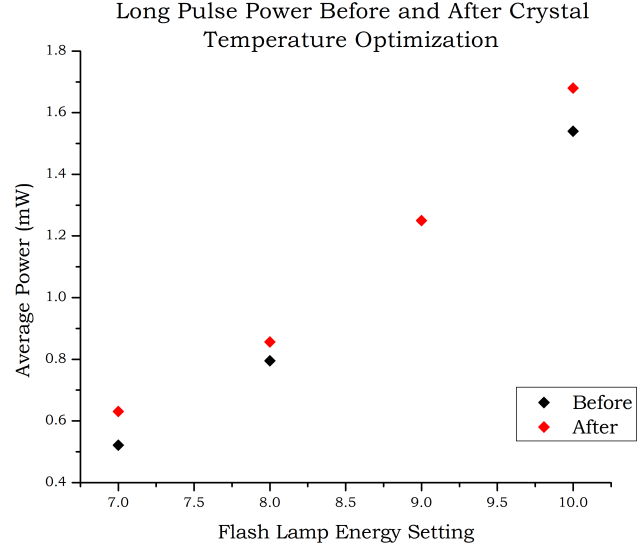
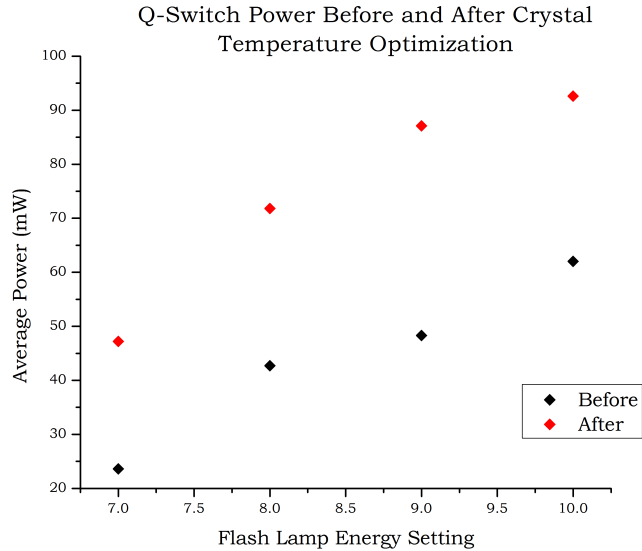


Figure 15: Using the areas of the peaks measured by the DataRay program, a temperature which outputted the peak power from the Nd:YAG laser could be calculated by fitting a Gaussian curve. The Gaussian curve had an R^2 value of .9525 and the peak power was found at a relative temperature of $-.893 \pm .124$, or .893 turns to the left.

The peak of the fitted gaussian curve provides the temperature setting for the crystal at which the highest amount of power is outputted from the laser. This occurred at a relative temperature of $-.893 \pm .124$, or .893 turns to the left. After changing the temperature setting to the optimal point, the average power outputted in both the long pulse and Q-SW settings of the laser were compared to the power before the optimization (Figure 16).



(a)



(b)

Figure 16: Before and after the crystal was set to the temperature found from Figure 15, the average power in both long pulse and Q-SW modes was measured. Figure 11(a) shows the results of the long pulse power changes and Figure 11(b) shows the same for the Q-SW mode.

As seen from the graphs, the power increased in both cases. In the Q-SW setting (Figure 11(b)), which is the more important setting for the application in this research, the power, on average, increased 75.5%. Thus, the temperature optimization was successful.

3.2.2 Pulse Width

Using an avalanche photodetector, Thorlabs APD110A, the pulse width of the Nd:YAG was measured. Connecting the APD110A to an oscilloscope, the voltage vs. time data was averaged over 20 pulses for pulse repetition rates (a setting on the Nd:YAG) of 1 Hz - 10 Hz. Analyzing this data with the computer data analysis program Origin, Gaussian curves were fitted for each set of data and the width of those curves were found. We then plotted pulse width as a function of repetition rate. We took data for both the Q-SW and the Long Pulse modes of the laser.

A pulse of the Nd:YAG in the long pulse setting is shown in Figure 17. Because this setting does not use the electro-optical Q-Switch discussed in section 3.1.3, lasing will occur as the crystal absorbs the energy from the flashlamp and emits photons. Figure 17 displays a single pulse from the Long Pulse setting. The spikes within the pulse indicate where the laser was lasing and the troughs are where the crystal was absorbing photons. There are 15 peaks. The duration from the beginning of the first to the end of the last is $35\mu\text{s}$. Thus the average time in between each spike is $1.83\mu\text{s}$. Another pulse had a length of $30\mu\text{s}$ and an average of $0.859\mu\text{s}$. These measurements give us information about the Nd:YAG crystal's absorption response time because the time between each spike is equal to the time period it took for the crystal to absorb and emit more photons. The duration of the pulse is on the same order as the average length of the flashlamp which is $\sim 200\mu\text{s}$.

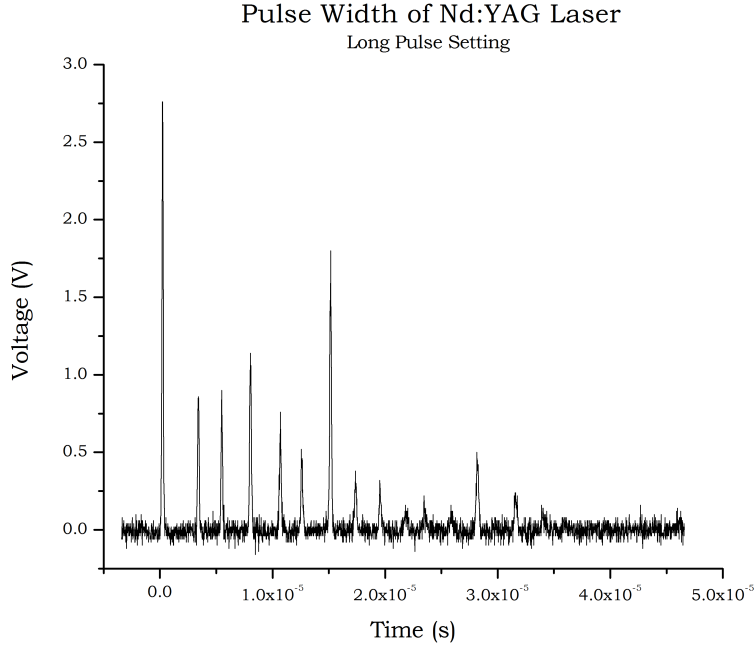


Figure 17: The pulse of the Nd:YAG laser in Long Pulse mode as measured by an avalanche APD photodiode and displayed on an oscilloscope. The intermittent peaks are due to the response time of the Nd:YAG crystal.

In Q-Switch mode, a pulse has a much more gaussian shape than the Long Pulse which we expect due to the electro-optical Q-Switch. A pulse is displayed in Figure 18. The Q-Switch data was much simpler to analyze because the pulse width is the width of a Gaussian curve fitted to the data.

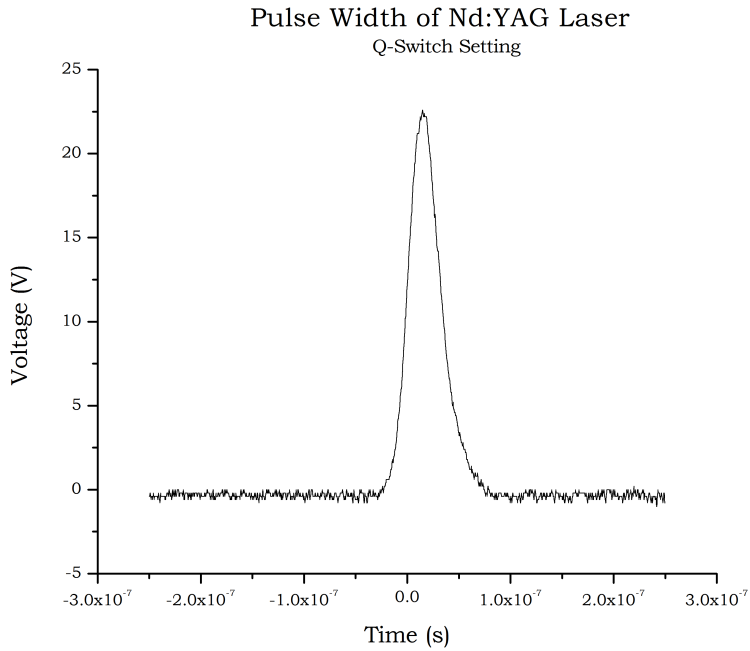


Figure 18: The Gaussian shape of a pulse in Q-SW mode on the Nd:YAG laser as measured by an APD photodiode and displayed on an oscilloscope. The pulse width of the peak is the width of a Gaussian fit to the data.

The pulse width versus repetition rate (Figure 19) yielded results with no trend. This means there is no dependence of the pulse width on the repetition rate. The average pulse width for the Q-SW mode was 33.5 ± 1 ns. The manufacturer's value for the pulse width is 6-7 ns. The reason for our discrepancy is the photodiode we used to detect the pulse width, Thorlabs APD110A, has a response time of 20 ns which is too slow to measure 6-7 ns and yields a broadening effect on our measured pulse width. Because of this, it is safe to assume our pulse width is < 33.2 nm and agrees with the manufacturer's value.

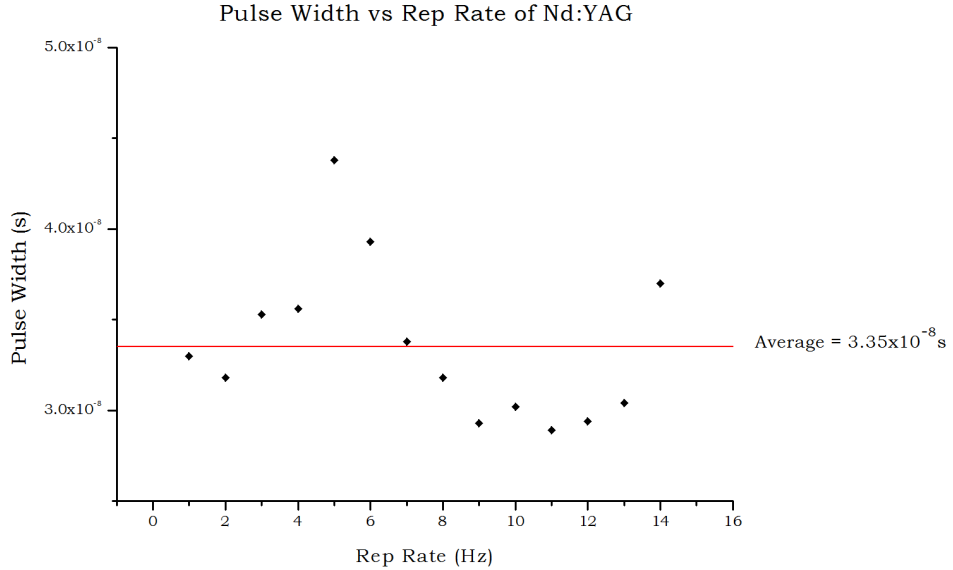


Figure 19: The pulse width of the Q-SW mode as a function of the repetition rate. The error bars for the data are smaller than the points themselves. There is no trend in the data which indicates there is no dependence. The average pulse width was found to be 33.5 ± 1 ns.

3.2.3 Power Output

Using a power meter specifically designed for pulsed lasers, we found the average power over 20 pulses as a function of flashlamp energy. We also recorded how the peak power of each pulse varies from pulse to pulse. We expected fluctuations in the pulse energy due to statistical differences in the cavity during each pulse, but extreme differences will make it difficult to efficiently pump the dye solution and could indicate that there is a problem with the Nd:YAG laser.

Power measurements of the Nd:YAG beam are found in Table 1 and displayed in Figure 20. Because the laser does not have enough energy to operate unless that flashlamp energy is set to above 6 for the Long Pulse mode and above 7 for the Q-Switch mode, data was only taken for flashlamp energies 7 and above. As one would expect, the Q-SW mode has a much higher peak energy, around 55.12 times larger, than that of the Long Pulse mode.

Flashlamp Energy Setting	LP Power (mW)	Q-SW Power (mW)
7	0.631±.001	47.2±.1
8	0.856±.001	71.8±.1
9	1.25±.001	87.1±.1
10	1.68±.001	92.6±.1

Table 1: Average power measurements for both Long Pulse and Q-SW modes over 20 pulses from the Nd:YAG laser at different flashlamp energies.

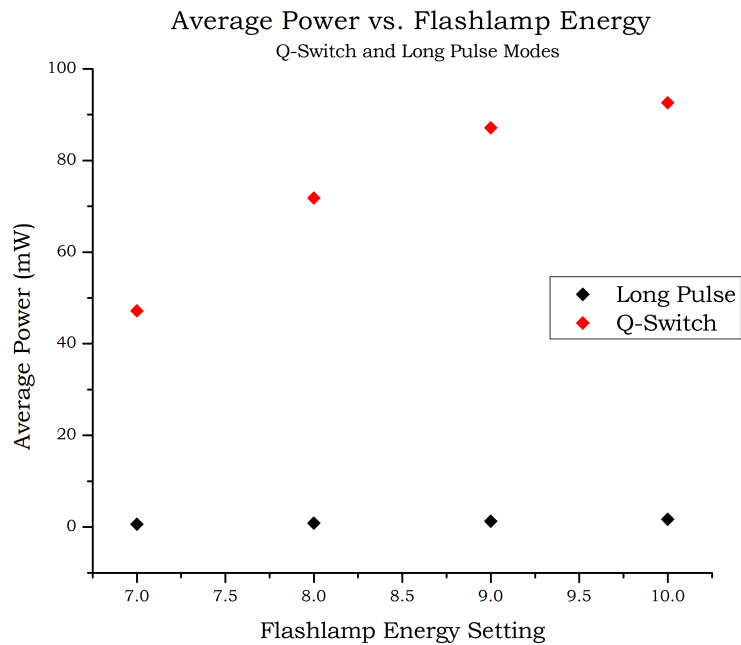


Figure 20: The average output power from the Nd:YAG laser as a function of flashlamp energy. Both modes increase as flashlamp energy increases, but in the Q-SW mode the power is much greater and thus is more noticeable in the graph.

We also notice a linear relation between output power and flashlamp energy. The slope of this linear relation is 15.15 ± 3.02 mW per flashlamp energy setting for the Q-Switched setting and $.354 \pm .034$ mW per flashlamp energy setting for the Long Pulse setting. Thus, the output power of the Q-SW mode increases much more rapidly than the Long Pulse mode.

4 Dye Laser

4.1 A Theoretical Understanding

4.1.1 Dye Molecules

A dye laser is characterized by a pump laser or other energy source that is aimed into a cell containing a dye solution which acts as the host medium for the laser. The liquid solution is made of a dye (organic molecules) and a solvent, usually water or alcohol. The significant characteristic of dye molecules is their structure. Their base consists of long chains of carbon-carbon bonds which alternate between single and double bonds (Figure 21).

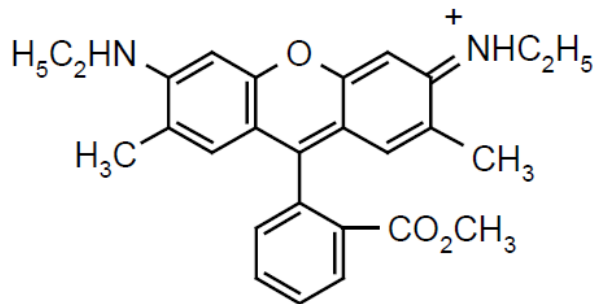


Figure 21: The molecular structure of Rhodamine 590 which is made of a long chain of conjugated double bonds [21].

The bonds between the carbon atoms are located on a plane. Above and below this plane, the π -orbitals of the carbon atoms overlap. This results in a delocalization of electrons which can then be approximated as particles in a one-dimensional potential square well. This well has a length, L , equal to the length of the carbon-carbon chain. With this, the energy of the n -th level of the square well can

be written

$$E_n = \left(\frac{\pi^2 \hbar^2}{2m_e L^2} \right) n^2 \quad [18] \quad (16)$$

where n is the energy level, E_n is the energy of that level, m_e is the mass of an electron, and L is the length as mentioned earlier. As stimulated emission of the dye molecule first requires absorption, the principle absorption energy is important. This can be calculated as the difference between energy levels E_n and E_{n+1} ,

$$\Delta E = \left(\frac{\pi^2 \hbar^2}{2m_e L^2} \right) n^2 - \left(\frac{\pi^2 \hbar^2}{2m_e L^2} \right) (n+1)^2 = (2n+1) \frac{\hbar^2}{8m_e L^2} \quad [18]. \quad (17)$$

The wavelength of such a transition can be found using $E = h\nu = \frac{hc}{\lambda}$. Substituting the result from equation 17 we find,

$$(2n+1) \frac{\hbar^2}{8m_e L^2} = \frac{hc}{\lambda} \quad (18)$$

And the wavelength is,

$$\lambda = \frac{8m_e c}{h} \frac{L^2}{2n+1} \quad [18]. \quad (19)$$

Because bond lengths for different molecules are known, L can be calculated. And, because the wavelength is directly proportional to this length, the longer the chain of molecules the longer the wavelength of principle absorption. With this feature, dye molecules have a large, and predictable, range of absorption and emission spectra and can be chosen for a specific wavelength range. A single dye typically has an operating range of 20-100 nm [18].

As two atoms get closer or form a bond, there are many more sub-levels within each distinct atomic energy level due to the rotational and vibrational states of the bond. This broad level shape is seen in Figure 22.

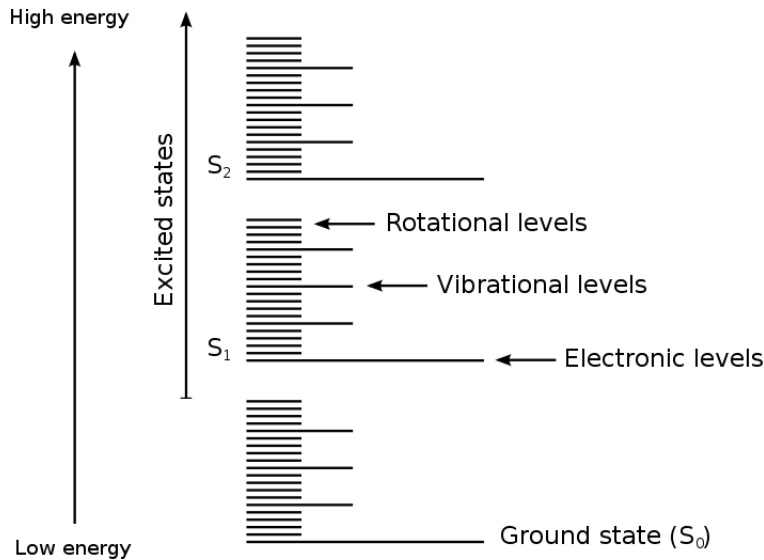


Figure 22: The broad shape of the energy levels of a molecule. There are many vibrational and rotational levels within each electronic level. This leads to many possible lasing transitions [22].

Electromagnetic radiation can excite a molecule into a rotational or vibrational state within a higher energetic state. These transitions are predicted by Franck-Condon factors, as discussed in section 5.2. For example, imagine a photon excites a molecule into an excited electro-vibrational molecular state of E_1 from E_0 . The molecule will spontaneously decay to the lowest vibrational state of E_1 . This is an internal, non-radiative decay. Next, the molecule will decay to the lower energy state E_0 . This decay is radiative and the energy is released in the form of a light pulse. Because the dye is made of large amounts of the same molecule, the result of exciting each molecule with equal energy photons (the pump beam is coherent) is equivalent energy pulses from each radiative decay and thus a new output laser. Population inversion is fairly easy to achieve in dye molecules because of the large number of vibrational and rotational states.

The dye is circulated through a quartz glass cell by a circulator, which also contains a reservoir of dye. The circulator replenishes old dye with new dye continuously. This prevents overheating and photobleaching of the dye. Photobleaching occurs when a transition to a lower energy state decays into a triplet state of the molecule. When the molecule is in a triplet state, there is a higher chance (due to the lifetime of the state) that it will react with other molecules in the en-

vironment. This may result in chemical damage of the molecules and thus optical quality can be lost [23]. Statistically, molecules spontaneously decay to triplet states very rarely, but over time it becomes a problem. Circulating the dye is one way to help avoid this issue.

As the dye circulates, it is pumped transversely by the pump source. If the size of the pump beam is smaller than the width of the dye cell (Figure 23(a)), emission from this area may be absorbed by the surrounding dye, thus inhibiting any exterior lasing. To counter this, a lens is used to broaden the beam and illuminate the entirety of the cell. Another lens focuses this broadened beam down into a horizontal line across the width of the cell in order to maximize the output power of the dye laser along that axis (Figure 23(b)).

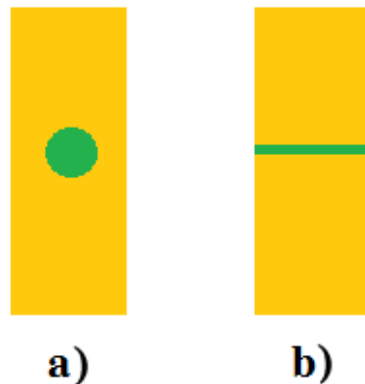


Figure 23: If the pump beam is aimed on the dye cell and it does not cover the width of the cell (a), the dye molecules surrounding the beam may absorb any lasing. Thus, it is necessary to use lenses to broaden the beam and focus it along the horizontal axis of the cell (b).

The cell must also be tilted at an angle away from the vertical in order to prevent reflections between the sides of the dye cell from creating a resonance cavity, as this would prevent control over the output beam (Figure 24).

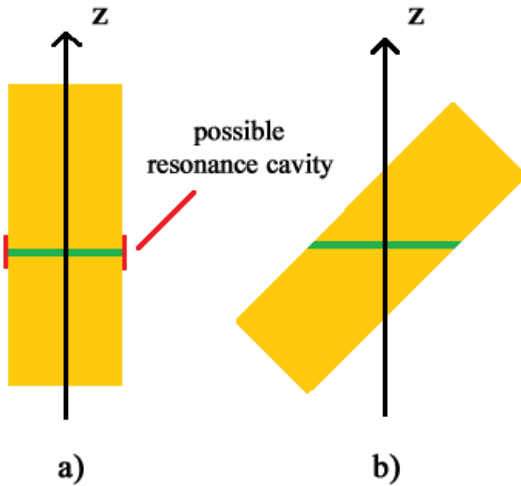


Figure 24: In order to prevent the side of the dye cell from creating a resonance cavity (a), the dye cell is tilted away from the vertical (b).

There are many advantages to having a liquid as the medium for a laser. Overheating and triplet state build up can be reduced by the circulation of new dye into the cell. This is coupled with the fact that circulated dye can also be cooled externally when not present in the cell. As photobleaching is decreased, the dye has a fairly long lifespan. All of these factors contribute to an ability to have a consistently high output power from the dye's fluorescence.

4.1.2 Laser Cavity

In order to amplify the light emitted by the dye, an external cavity is used to oscillate the new beam repeatedly back through the dye to increase stimulated emission. There are a few different geometries one can use to make a dye laser. We decided to use the scheme outlined by Littman and Metcalf in their paper, “Spectrally narrow pulsed dye laser without beam expander” [24].

This cavity includes two mirrors, the dye cell, and a diffraction grating. A diagram can be seen in Figure 25.

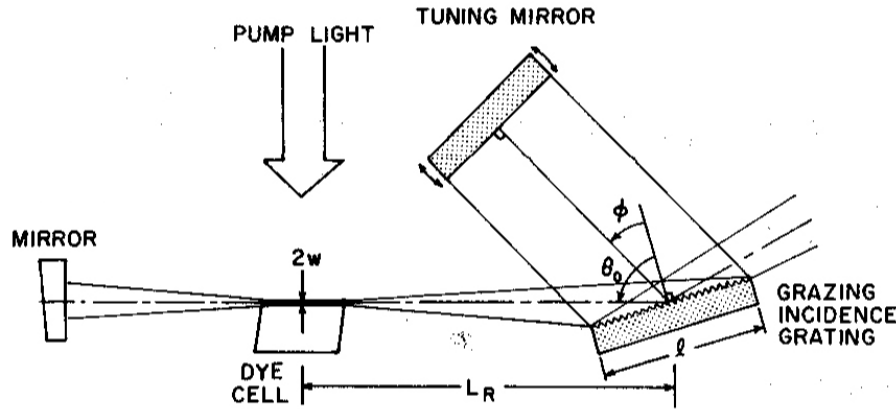


Figure 25: Littman and Metcalf's cavity design. The design uses two mirrors and a diffraction grating to create the cavity which oscillates the light back and forth through the dye cell. The top mirror is the tuning mirror and the output beam is the 0th order of the diffraction grating. This is advantageous as the output beam has a fixed direction even while the beam is tuned [24].

As the dye is transversely pumped, it emits amplified spontaneous emission in all directions. In order to create stimulated emission in a chosen resonant mode and along a particular axis, a mirror and a diffraction grating are placed on either side of the dye cell perpendicular to the pump beam. The 1st order reflection off the diffraction grating is reflected back onto the grating using another mirror placed in front of it. This reflection is what creates the closed cavity as it will be directed back through the dye cell and onto the other mirror. This oscillation will continue within the cavity producing an amplified beam. The output beam is the 0th order of the diffraction grating. The tuning component of this cavity setup is the mirror reflecting the 1st order back onto the grating. By changing the angle of this mirror, we can change the wavelength. Littman and Metcalf described the relation with the equation

$$m\lambda = a(\sin(\theta) + \sin(\phi)) \quad [24], \quad (20)$$

where m is the diffraction order, λ is the wavelength of the output beam, a is the groove spacing of the diffraction grating, θ is the angle of incidence and ϕ is the angle between the normals of the grating and tuning mirrors (Figure 26). Thus, holding everything else constant

and changing ϕ we can tune the wavelength of the dye laser. The advantage of this is that the output beam will not change direction as the wavelength is tuned, it will stay fixed in the direction of the 0th order of the diffraction grating.

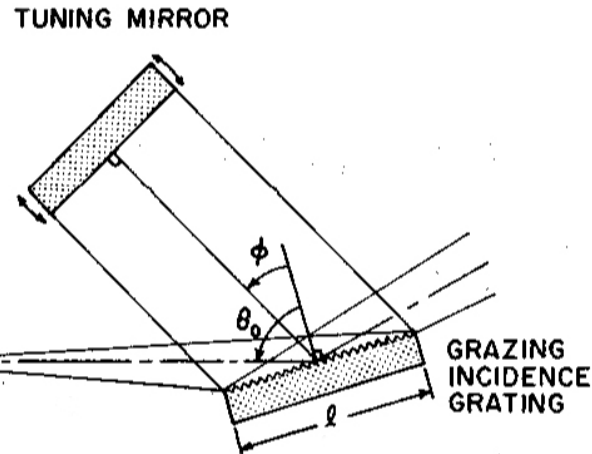


Figure 26: A close up on the tuning mirror of the Littman and Metcalf configuration seen in Figure 25. The angles represented give an equation (Equation (20)) for calculating the wavelength [24].

4.2 Cavity Construction

The dye laser is located on an optical table. After filtering out the 1064 nm light, the pump laser points into a converging lens with a focal length of +175 mm. This lens was placed 17 cm from the second dichroic mirror and is used to broaden the beam before it is incident on the dye cell. This insures the beam covers the width of the cell as mentioned earlier. Next, a cylindrical lens with a focal length of 100mm, Thorlabs LJ1567L1-A, focuses the light along the horizontal axis of the rectangular quartz cell (12.5 mm x 45 mm x 12.5 mm) containing the dye solution, as seen in Figure 23. This lens is located 42 cm from the converging lens. Once the beam has passed through the cylindrical lens, it travels 15.5 cm to the dye cell. Before constructing the cavity around the cell, we first gauranteed that the two mirrors and the diffraction grating were completely flat by reflecting a HeNe laser off their surfaces and adjusting the angle knobs until the laser was directed back to its source. Once this was achieved, we placed a

silver coated mirror and a diffraction grating on either side of the dye cell. A picture of the resonance cavity is shown in Figure 27.

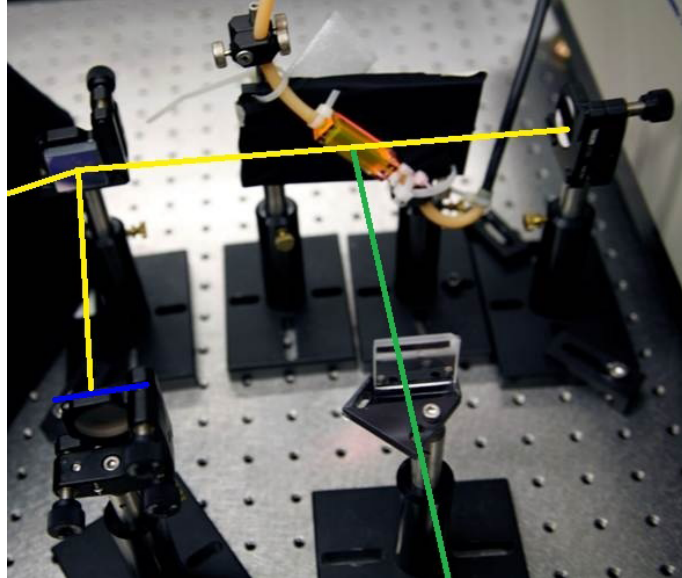


Figure 27: A picture of our dye cell cavity. The pump light (green line) is incident on the dye cell. The diffraction grating and a mirror are placed on either side of the cell and the tuning mirror is located in front of the diffraction grating. The lasing light from the dye follows the yellow lines.

The diffraction grating we used is a Thorlabs grating with 1800 lines per mm and a blaze angle of 500 nm. Both the mirror and grating are 10 cm away from the dye cell and along the same axis the pump source was focused onto. To complete the cavity, we positioned the tuning mirror 6.5 cm in front of the diffraction grating where the first order reflection occurred. Locking down the diffraction grating, we fixed the direction of the output beam. Next, using an iris, we guaranteed the beam was reflecting off the tuning mirror back onto the diffraction grating and back through the dye cell to create the cavity. The dye, Rhodamin-590, is in solution with methanol and continuously circulated through the cell by the circulator. It has a molar concentration of $2.5 \times 10^{-4} \frac{\text{mol}}{\text{L}}$. A photo of the entire setup is shown in Figure 28.

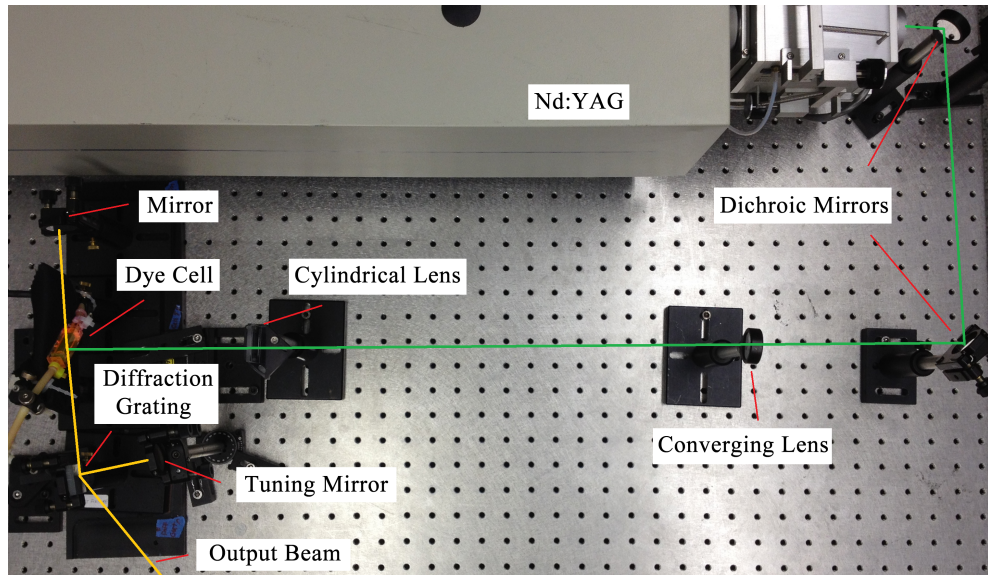


Figure 28: A photo of the entire setup of the dye laser. The green lines indicate the pump laser and the yellow show where the path of the dye laser is.

4.3 Characterization of the Dye Laser

Once the system was lasing, we characterized the output beam of the dye laser. Using a spectroscope made by Ocean Optics, we measured the intensity. We noticed two peaks at different wavelengths. Because we expect a single wavelength output from the dye, this second peak corresponds to the amplified spontaneous emission of the dye that occurs without the resonance cavity. Using the spectroscope, we were able to reduce the peak by adjusting the angles of the mirrors and the diffraction grating to ensure all of the lasing light oscillates within the Littman-Metcalf cavity before exiting. We were also able to maximize the output power as the intensity is proportional to the power.

Next, we measured the power using both the spectroscope and a power meter, both averaged over 20 pulses. We plotted these measurements and fit a Gaussian curve to find the maximum intensity. We found the peak power of the dye laser and at which wavelength this occurred.

We found the wavelength range of the dye laser to be 559-596 nm. When measured on the power meter, the peak power was measured at $572.4 \pm .4$ nm (Figure 29). And the R^2 value for the fit was .966.

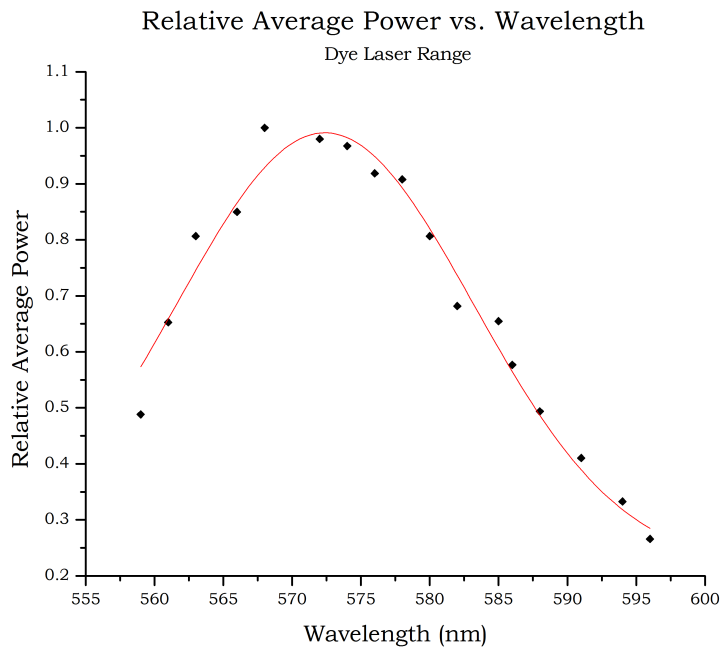


Figure 29: Averaged over 20 pulses, the relative average power of the dye laser had a maximum at $572.4 \pm .4$ nm.

Comparatively, when using the spectroscope, the peak power occurred at $579.7 \pm .5$ nm (Figure 30). The R^2 value for the gaussian fit was .975. When using the spectroscope, we noticed an abnormal pulse shape (shown in Figure 31) that was not consistent for all the output wavelengths, it increased as the wavelengths got larger. This could shift the maximum to larger than the true value.

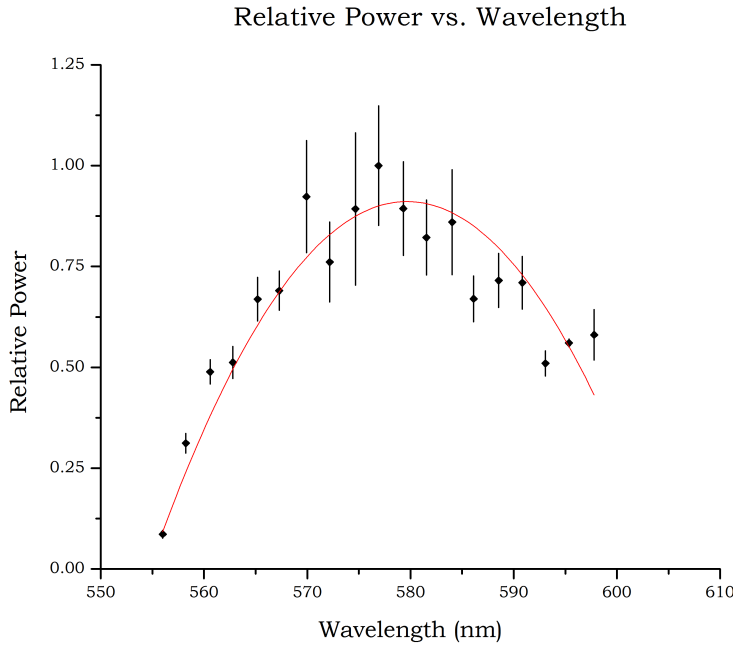


Figure 30: Using the spectroscope we were able to measure intensity as a function of wavelength. As intensity is proportional to power, this is also a measurement of relative power. The peak power was measured at $579.7 \pm .5$ nm.

The literature value for the range of Rhodamine 590 with a molar concentration of $2.2 \times 10^{-4} \frac{\text{mol}}{\text{L}}$ in methanol and pumped by an Nd:YAG laser is 552-580 nm with a peak at 560 nm [21]. The concentration of our dye is $2.5 \times 10^{-4} \frac{\text{mol}}{\text{L}}$ which is a higher concentration. Methanol also evaporates over time increasing this concentration even more. This could attributed to the discrepancy between our measured values and the literature values. Literature values for higher concentrations ($6 \times 10^{-4} \frac{\text{mol}}{\text{L}}$) are shifted higher into ranges such as 563-597 nm with a peak at 574 nm [21]. These numbers agree more with our measured values from the power meter (559-596 nm, 574.2 nm). The largest peak value for any concentration was 578 nm [21]. Thus, the peak power of the spectroscope, $579.7 \pm .5$ nm does not agree with literature values. This could be due to the abnormal pulse shapes mentioned previously and shown in Figure 31.

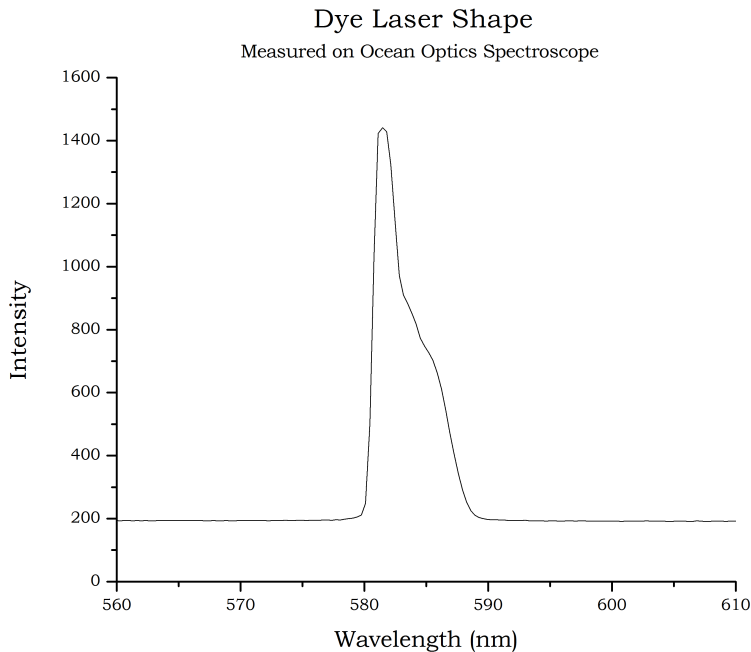


Figure 31: A pulse of the dye laser as measured on the spectroscope. The peak is not a Gaussian shape which we expected. The abnormal shape is more pronounced at higher wavelengths and thus could shift the peak power to a higher wavelength than the true value.

5 Application and Outlook

5.1 Ionization of Ultracold RbCa

Now that the dye laser has been constructed, it will be used in research studying ultracold RbCa. Specifically, it will be used in a process known as REMPI (Resonantly Enhanced Multi-Photon Ionization). REMPI is a way to determine the number of RbCa molecules created within the MOT as well as the quantum energy states of the RbCa molecules. Photo-ionization occurs when a molecule absorbs multiple photons with enough combined energy to free an electron, essentially to eject it free of the electromagnetic forces of the molecule. In this experiment, this will occur with two photons, one after another. If the energy of the first photon is equal to the energy difference between the original energy state of the molecule and a higher vibra-

tional level, an excitation will occur. A second photon incident on the excited molecule will then knock the excited electron free, ionizing the molecule and creating RbCa^+ (Figure 32).

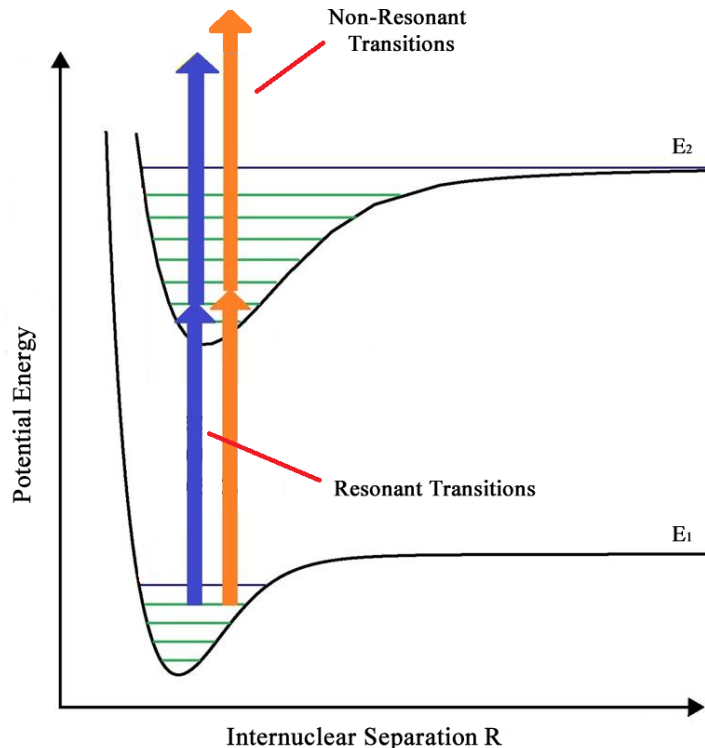


Figure 32: A diagram of the energy levels of a molecule and the process of REMPI (Resonantly Enhanced Multi-Photon Ionization) which creates an ion. If the photons have energy equal to the difference between the energy levels (left pair of arrows), the transition will be more favorable than the right set of arrows which depict non-resonant photons. The first photon excites the electron to a higher level and the second photon ionizes the molecule by ejecting the electron free of the electromagnetic force of the atom [4].

By ionizing the molecules using the dye laser, they can be more easily detected using time-of-flight spectroscopy. Time-of-flight spectroscopy uses electric fields to move ions towards a detector. In an electric field, the kinetic energy of a charge q can be written,

$$qU = \frac{1}{2}mv^2 . \quad (21)$$

In an ion, q becomes the charge of the extra proton, $q = e$. The potential energy of an electric field can be written $U = \frac{\Delta V}{d}$ where ΔV is the potential difference and d is the distance between the electrodes. Then equation 22 becomes,

$$e \frac{\Delta V}{d} = \frac{1}{2}mv^2 . \quad (22)$$

If we write $v = \frac{\Delta x}{\Delta t}$ and solve for Δt we find,

$$\Delta t = \sqrt{\frac{d * m}{2\Delta V}} \Delta x . \quad (23)$$

Because ΔV , d , Δx are all known and can be fixed, m is the variable which time is dependent on. Thus, larger ions will take longer to travel a distance d . With this, RbCa can be differentiated from any other molecules. The detector will display the count of ions created over time.

Because the nature of molecules is fundamentally quantum, the energy differences between the different energy levels is an important characteristic to measure. Using time-of-flight spectroscopy and the tunable dye laser, we can measure exactly these. As governed by the Franck Condon factors discussed in section 5.2, certain energy level transitions are more favorable and thus more ions will be created by the dye laser when its energy is resonant with these levels. By knowing the energy of the dye laser when the resonant transitions to ionization occurred, we can gain information about the location of these states. The energy of the dye laser can be slowly tuned to different values while detecting the counts of ionized molecules. An example of expected results can be seen in Figure 33 which was taken from a paper entitled “Spectroscopy of K₂Rb triplet excited states using ultracold state molecules formed by photoassociation” by J.T. Kim *et al.* [25].

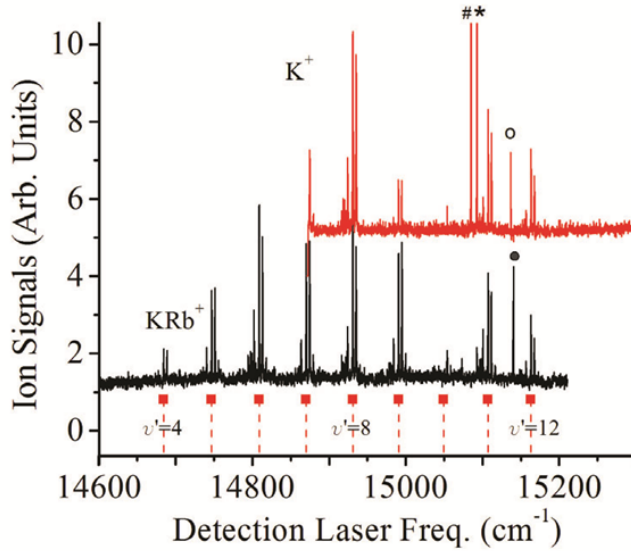


Figure 33: A graph of the ion signal versus the frequency of the dye laser. The spikes indicate more favorable ionization, which also corresponds to the dye laser being resonant with an energy level transition. Because this occurs at distinct energy values, the energy of the dye laser at these spikes is the same as the energy of that level. Thus a lot of information is gained from tuning the dye laser over a range of wavelengths. This is the type of data this experiment hopes to collect in the future [25].

This graph shows ion counts as a function of the detection laser frequency, in our case the detection laser will be the dye laser. The spikes indicate large amounts of ion formation and thus where the detection laser was in resonance between two molecular energy levels. The peaks are grouped around the energetic levels and each peak indicates where a rotational or vibrational level exists within that energetic level.

5.2 Franck Condon Principle

The Franck Condon Principle describes the energetic transitions of molecules which are more complicated than singular atom systems.

Molecules have four contributions to their total energy: electronic energy, vibrational energy, rotational energy, and translational energy. If translational energy is assumed to be zero, a safe assumption when working in the ultracold regime, the focus can be placed on the quantum structure. Due to the difference in mass of the electron and the nuclei, electronic transitions occur far more quickly than the Coulomb force's reactions to them in the nuclei [26]. Thus, the nuclei can be considered to be stationary during the transition. This allows relatively simple calculations of permitted transitions. Because the electronic transition is so fast, transitions are more favorable when the least change in the nuclear coordinates occurs. The energy levels, vibrational levels, and the wave functions for each can be represented as a vertical ladder within potential wells for each electronic energy (Figure 34). Levels that are directly above the original state will have the least change in nuclear coordinates and will thus be more probable. When considering a diatomic system, the nuclear coordinates become the single variable R , the separation between the two nuclei.

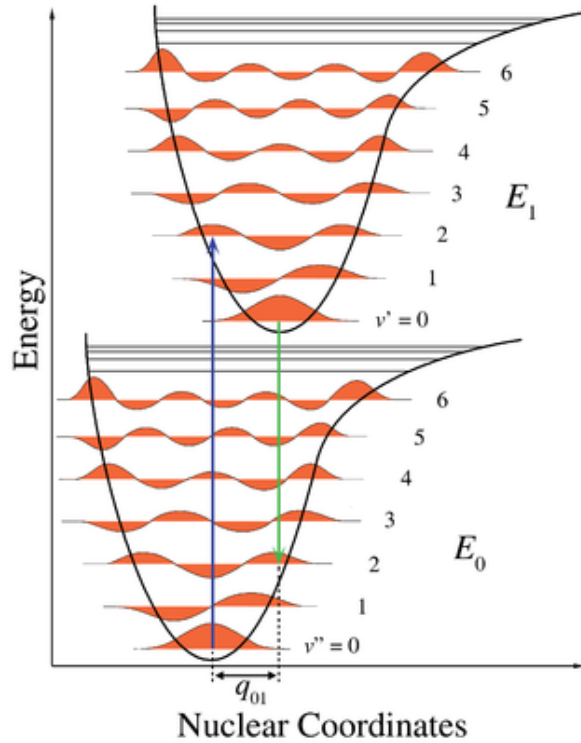


Figure 34: The wavefunctions of an electron at different vibrational states within the ground and first excited energy states. The change in nuclear coordinates as well as the overlap of the wavefunctions determines the probability of a transition occurring. This probability is known as the Franck-Condon Factor. The arrows indicate a probable absorption and a probable decay [27].

Also contributing to the likelihood of a transition is the overlap between the two wavefunctions associated with the transition states. This value, also known as the Franck-Condon Factor, can be expressed mathematically as

$$f_{\nu'\nu''} = \left| \int_0^{\infty} \Psi_{\nu'} \Psi_{\nu''}^* dR \right|^2, \quad (24)$$

where $f_{\nu'\nu''}$ is the Franck-Condon factor, $\Psi_{\nu'}$ is the wavefunction of the upper level and $\Psi_{\nu''}$ is the wavefunction of the lower level. The larger the Franck-Condon Factor is, the more likely the transition will occur.

Using the Schrödinger equation, calculations of the wavefunctions

for all of the electronic and ro-vibrational states of the diatomic molecule RbCa were determined. From these wavefunctions, and using LEVEL 8.0 [28], the Franck-Condon factors for all possible transitions within the molecule were calculated. In Figure 35 the potential energy functions of the energy levels of RbCa are plotted. The functions of the second excited state and the third excited state are the same. Similarly, the functions of the fourth excited state and the fifth excited state are the same.

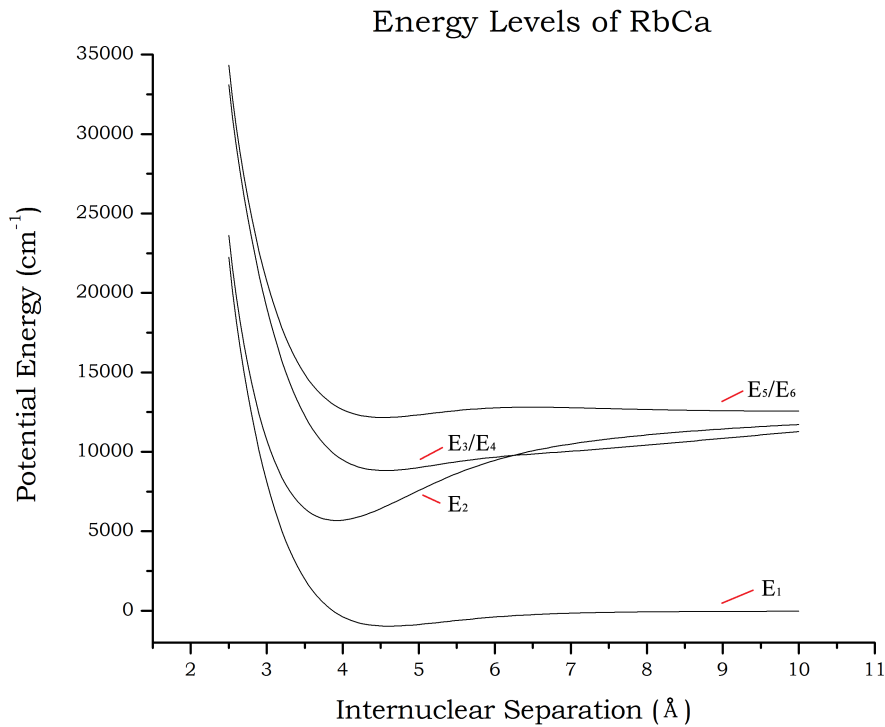


Figure 35: The potential energy functions of the energy levels of RbCa. Because the second and third states have the same function and the fourth and fifth do also, there are four potential wells.

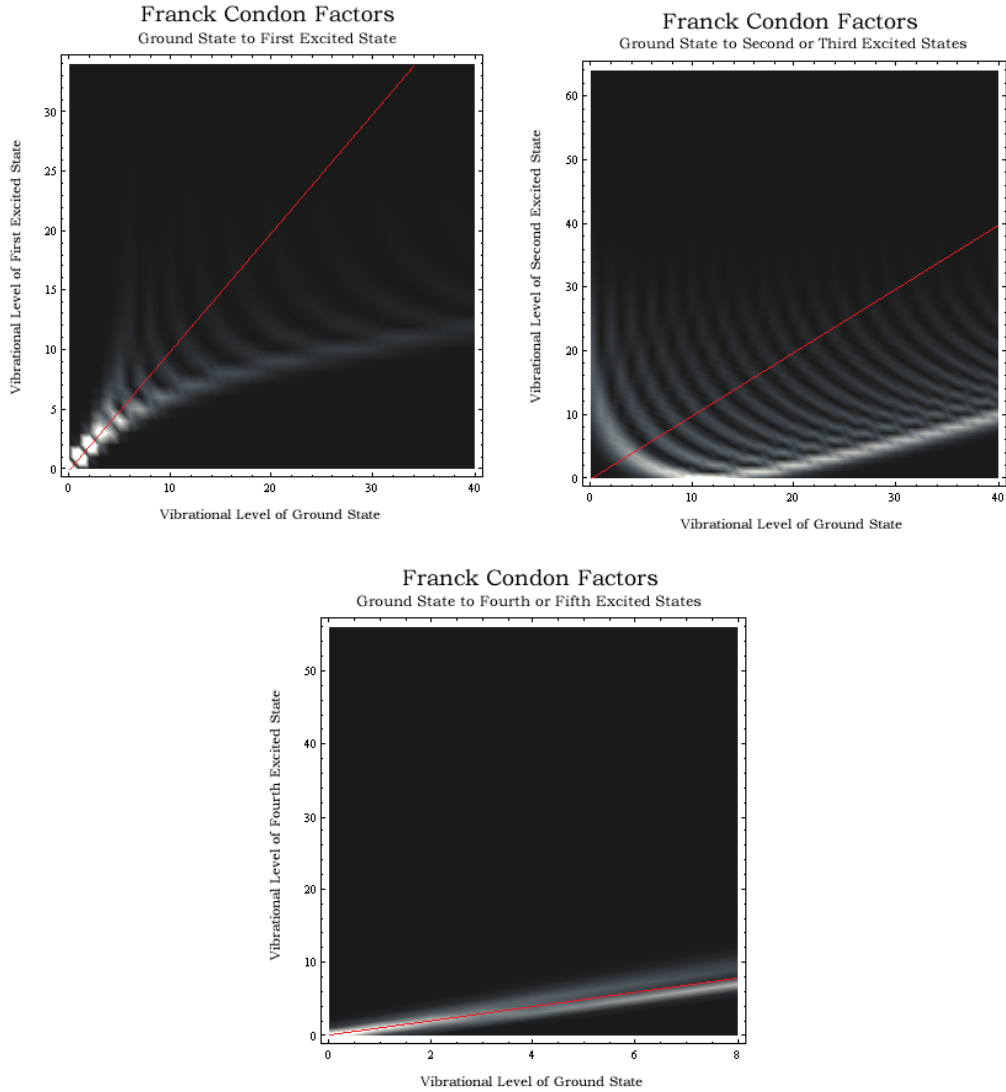


Figure 36: The density plots of the Franck-Condon factors for transitions from the ground state of RbCa to the first, second, third, fourth and fifth excited levels. The red lines show the symmetry of the vibrational states. Because the ground state to the first excited state has strong Franck-Condon factors along this linear relation, these transitions would be probable and easier to control.

In Figure 36 the density plots of the Franck-Condon factors for

the ground state to the first, second, third, fourth, and fifth excited states are plotted. The red lines show the symmetry of the vibrational levels between the two energetic levels. Because the ground state to the first excited state has strong Franck-Condon factors along this linear relation, these transitions will be much more probable. To have a starting point when attempting to ionize ultracold RbCa, we choose the strongest Franck-Condon factor as its transition will be very favorable. Table 2 displays the three largest Franck-Condon factors for transitions between the ground state and the first, second, third, fourth, and fifth excited states. The largest Franck-Condon factor occurred between the 0th vibrational level of the ground state and the 0th vibrational level of the first excited state. This had a Franck-Condon factor of 0.988401 which means the wavefunctions of these levels were only 1.16% different. Thus, this transition is a great starting point to use as the wavelength of the dye laser because the transitions to ionization will be very favorable.

Franck-Condon Factor Transition Vibrational Levels ($\nu' - \nu''$)	
Ground State to First Excited State	
.988401	0 - 0
.933018	1 - 1
.781926	2 - 2
Ground State to Second Excited State	
.130305	11 - 0
.126043	12 - 0
.121007	10 - 0
Ground State to Third Excited State	
.148299	0 - 10
.138960	0 - 11
.138101	0 - 9
Ground State to Fourth Excited State	
.887952	0 - 0
.686164	1 - 1
.515876	2 - 2
Ground State to Fifth Excited State	
.980142	0 - 0
.950652	1 - 1
.930821	2 - 2

Table 2: Three largest Franck-Condon factors for the transition between the ground state to the first, second, third, fourth, and fifth excited states. The left column displays the Franck-Condon factor and the right has the vibrational levels the factor corresponds to.

In order to tune the dye laser to the correct frequency for this transition to occur, we begin with the dye laser tuned to a frequency, f_1 , and reduce it to another frequency, f_2 . f_1 is proportional to the energy difference between the ground and excited states when the internuclear separation is large ($\sim 10\text{\AA}$) which we will call E_1 . This energy value is $E_1 \sim 1,150,000 \text{ m}^{-1}$. f_2 is proportional to the energy difference for the chosen transition, the 0th vibrational level of the ground state and the 0th vibrational level of the first excited state. This energy difference has a value of $E_2 = 1,007,857 \text{ m}^{-1}$. The change in energy thus is

$$E_2 - E_1 = 1,150,000 - 1,007,857 = 142,143 \text{ m}^{-1}. \quad (25)$$

Using the Planck relation, we convert this into a frequency and find the necessary change in frequency of the dye laser for this transition to be 42.6134 THz.

Once the molecules have been cooled in their respective traps and the molecules have been formed, the dye laser will now be ready to ionize them and help add to this ever growing and exciting field.

References

- [1] S. Bose, “Planck’s law and the hypothesis of light quanta,” *Zeitschrift fur Physik*, vol. 26, pp. 178–181, 1924.
- [2] W. Phillips, C. Tannoudji, and S. Chu, “The manipulation of neutral particles,” *Reviews of Modern Physics*, vol. 70, no. 3, 1998.
- [3] M. Anderson, J. Ensher, M. Mathews, C. Wieman, and E. Cornell, “Observation of bose-einstein condensation in a dilute atomic vapor,” *Science*, vol. 269, pp. 198–201, 1995.
- [4] J. Zhong-Hua, Z. Hong-Shan, W. Ji-Zhou, Y. Jin-Peng, Z. Yan-Ting, M. Jie, W. Li-Rong, X. Lian-Tuan, and J. Suo-Tang, “Photoassociative production and detection of ultracold polar rbcs,” *Chinese Physics Letters*, vol. 28, no. 8, 2011.
- [5] K. Ni, S. Ospelkaus, D. Nesbitt, J. Ye, , and D. Jin, “A dipolar gas of ultracold molecules,” *Physical Chemistry and Chemical Physics*, vol. 11, no. 42, pp. 9626–9639, 2009.
- [6] D. Jaksch, “Optical lattices, ultracold atoms and quantum information processing,” *Contemporary Physics*, vol. 45, no. 5, pp. 367–381, 2004.

- [7] P. Sorokin, J. Lankard, E. Hammond, and V. Morruzi, "Laser pumped stimulated emission of organic dyes: experimental studies and analytical comparisons," *IBM Journal of Research and Development*, vol. 11, no. 2, pp. 130–148, 1967.
- [8] <http://www.nobelprize.org/educational/physics/laser/facts/applications.html>. April, 2012.
- [9] <http://scientopia.org/blogs/skullsinthestars/2010/08/02/optics-basics-lasers/>. April 2012.
- [10] <http://www.ecse.rpi.edu/~schubert/Light-Emitting-Diodes-dot-org/chap14/chap14.htm>. April, 2012.
- [11] S. Orazio, *Principles of Lasers*. Plenum Press, 4th ed.
- [12] *Quanta Ray Instruction Manual*. Spectra Physics. Germany, 1992.
- [13] <http://www.star.le.ac.uk/~rw/courses/lect4313.html>. Dec, 2011.
- [14] *Lambdacrome Laser Dyes*. Lambda Physik USA, Inc., 3rd ed., 2000.
- [15] http://staff.aist.go.jp/narazaki-aiko/SHG_en.html. Dec, 2011.
- [16] <http://www.stanford.edu/group/scintillators/ceramicprocessing.html>. Feb, 2012.
- [17] http://www.rp-photonics.com/phase_matching.html. March, 2012.
- [18] S. Hooker and C. Webb, *Laser Physics*. Oxford University Press, 2010.
- [19] <http://www.u-optic.com/kdp.htm>. Feb, 2012.
- [20] *Win CamD Series, DataRay*. DataRay Inc. Bella Vista, CA, 2011.
- [21] <http://www.exciton.com/pdfs/RH590.pdf>. Dec, 2011.
- [22] https://commons.wikimedia.org/wiki/File:Molecular_energy_levels_en.svg. Dec, 2011.
- [23] <http://micro.magnet.fsu.edu/primer/java/fluorescence/photobleaching/>. April, 2012.
- [24] M. Littman and H. Metcalf, "Spectrally narrow pulsed dye laser without beam expander," *Applied Optics*, vol. 17, pp. 2224–2227, 1978.

- [25] E. E. E. P. L. G. J T Kim, D Wang and W. C. Stwalley, "Spectroscopy of kr₂ triplet excited states using ultracold state molecules formed by photoassociation," *New Journal of Physics*, vol. 11, 2009.
- [26] http://chemwiki.ucdavis.edu/Physical_Chemistry/Spectroscopy/Electronic_Spectroscopy/Franck-Condon_Principle. April, 2012.
- [27] http://en.wikipedia.org/wiki/Franck%20%80%93Condon_principle. Dec, 2011.
- [28] R. J. LeRoy, *LEVEL 8.0*. Guelph-Waterloo Centre for Graduate Work in Chemistry. University of Waterloo, Waterloo, Ontario, Canada, 2007.